Sensors and Actuators A 169 (2011) 124–132

Contents lists available at ScienceDirect

Sensors and Actuators A: Physical

journal homepage: www.elsevier.com/locate/sna

High performance Integrated Electro-Hydraulic Actuator for robotics. Part II: Theoretical modelling, simulation, control & comparison with real measurements*

Samer Alfayad[a], Fethi B. Ouezdou[a,*], Faycal Namoun[b], Gordon Cheng[c]

[a] Laboratoire d'Ingénierie des Systèmes de Versailles, EA 4042, 10-12 Avenue de l'Europe, 78140 Vélizy, France
[b] BIA, ZA Les Boutriers, 8 rue de l'Hautil, 78000 Conflans fin d'Oise, France
[c] Institute for Cognitive Systems, Technical University Munich, Munich, Germany

article info

Article history:
Received 14 July 2010
Accepted 16 October 2010
Available online 15 March 2011

Keywords:
Integrated actuator
Electro-hydraulic
Actuator modelling
Actuator control
Simulation

abstract

The paper deals with the theoretical modelling of the high performance Integrated Electro-Hydraulic Actuator (IEHA) introduced in the first part of this work. Based of the hydraulic and dynamic equations, we carried out an analysis of the IEHA input/output relation. A simulation based on this input/output model is detailed showing the ability to access several time derivatives of the payload position mainly its "jerk", which represents an important issue whenever motion control is considered. We show the theoretical dynamic properties of the proposed solution through open and closed loop simulation results based on Matlab-Simulink. A comparison between the theoretical and experimental results obtained by a built prototype is given in order to demonstrate the promising performances of the proposed solution.

1. Introduction

In the first part of this work [1], a novel Integrated Electro-Hydraulic Actuator (IEHA) was proposed. The IEHA is basically based on a technology named Hydrostatic Transmission, first proposed for robotic application by Bobrow et al. [2] and followed by Habibi who introduced the concept of ElectroHydraulic Actuator (EHA) [3]. In all hydraulic solutions for robotic applications [4–7], the hydraulic motor control and hence the pay-load or the positioning is carried out by controlling either a fixed or variable displacement pump rotation. In the case of a fixed displacement pump, a power control of the servo electric motor has to be carried out, leading to sophisticated control laws which limit the use of this kind of solution in high numbers system, such as humanoid robots. In the case of a variable displacement pump with a constant speed electric motor, a bidirectional pump is also needed leading to the necessity of inverting the electric motor direction, which induces the appearance of a dead-band, thus, a loss in the system's efficiency. Consequently, in all former solutions, power production is made instantaneously and the hydrostatic actuator has to be sized according to the worst-case constraints. Our approach in developing the IEHA was inspired by humans' behavior in their process of motion/force production. It is well known that the human being can achieve with their muscles two kinds of modes called isometric and isotonic [8]. For the isometric functioning, the link (arm or leg) has to keep a given position and to exert some force varying from zero (without contact with the environment) to a maximum value (contact force, pushing, pulling or propelling during locomotion gait). The force variation is ensured by the recruitment of muscular fibers with some electric activation signal. For the isotonic mode, the muscles are compensating the gravity effects and no more contraction (activation) is required to carry out smooth movement. In the IEHA proposed solution, a built-in micro-valve activated with a magnetic coil and controlled with a Linear Variable Differential Transformer (LVDT) sensor [9] is integrated in order to allow us to emulate the muscle's activation phenomena by changing the eccentricity of the micro-pump. Inverting the flow and the pressure direction by keeping the same rotation is carried out with a built-in rotary passive distributor, which has three possible positions depending on the pressure in the input and output lines of the micro-pump. The established mathematical model of the input/output relation shows the capacity of the system to access to the "jerk" of the pay-load and giving us the possibility to minimise it whenever carrying isotonic movements.

DOI of original article: 10.1016/j.sna.2010.10.026.
* A part of this paper has been presented at the 2009 IEEE International Conference on Robotics and Automation (ICRA 2009), Kobe, Japan.
* Corresponding author.
E-mail addresses: sfayad@hotmail.fr (S. Alfayad), ouezdou@lisv.uvsq.fr (F.B. Ouezdou), f.namoun@bia.fr (F. Namoun), gordon.cheng@ieee.org (G. Gheng).

0924-4247/$ – see front matter © 2011 Elsevier B.V. All rights reserved.
doi: 10.1016/j.sna.2011.03.019

Nomenclature

E	eccentricity (m)
S_p	piston surface (m^2)
Q	micro-pump average flow (m^3/min)
N_p	global pistons number (−)
	rotation speed (rpm)
P	fluid pressure (bar)
X	position of the micro-valve body (m)
Y	payload position (m)
R	theoretical micro-valve radius (m)
	micro-valve surface opening (m^2)
V_{P_b}	fluid velocity at point P_b (m/s^2)
V_{D_1}	fluid velocity at point D_1 (m/s^2)
	fluid volumic density (kg/m^3)
P_0	micro-valve fluid source pressure (bar)
	difference of the pressure created by the movement of the micro-valve (bar)
Q_e	flow created by the movement of the micro-valve (m^3/s)
C	Vena Contracta constant (−)
V_e	CH_{e1} chamber's volume (m^3)
	compressibility coefficient (bar^{-1})
S_v	active section of the linear actuator (m^2)
V_v	CH_v chamber's volume (m^3)
$\mathbb{F}_{e1}$, $\mathbb{F}_{e2}$	forces produced by the fluid of the micro-valve on the barrel (N)
$\mathbb{F}_{pi}$	force exerted by the i th piston at the barrel (N)
P_{vl}	CH_v chamber's pressure (bar)
P_{pi}	pressure of the i th piston (bar)
m_e	barrel mass (kg)
	barrel acceleration (m/s^2)
S_e	barrel active surface (m^2)
ω	rotation speed (rad/s)
V_{pi}	fluid velocity in chamber CH_{pi} (m/s)
L_0	linear actuator total length (m)
m	payload mass (kg)
F_c	external force applied to the payload (N)

This paper is organised as follows: in Section 2, the proposed IEHA input–output relationship is developed. Based on this theoretical model, a simulation tool using Matlab-Simulink is carried out in the third section. Finally, comparisons between theoretical and experimental results are detailed and further developments of this work are given.

2. IEHA input–output relationship

In this section, the relationship of IEHA input–output is established. This relationship is linked to the input, the position X of the micro-valve body to the payload position Y in the case of a linear actuator. The same relationship can be established even if a rotary hydraulic actuator is used. In this case, the input–output is linked to X with the angular position () of the actuator. Fig. 1 shows a simplified sketch of a planar section of the proposed IEHA, as in the case of a linear actuator. Based on these relationships, models of the different stages of the IHEA can be established. We start the modelling process with the micro-valve stage, as it controls the input signal X. Then, the equation of motion of the micro-pump barrel is established using the average flow calculation given by the following equation:

$$Q = 2N_p E S_p Q \tag{1}$$

where N_p the total number of pistons, E is the eccentricity of the micro-pump, S_p is the surface of one piston and is the rotation speed of the input shaft. A microscopic study to quantify the amount of each piston contribution can be carried out, in order to provide a better approximation of the dynamic effects applied to the micro-pump barrel. Lastly, we model the final stage of the process, which deals with the dynamics of the linear actuator driving the payload.

2.1. Micro-valve equation of motion

The opening, , allows the fluid passage is defined by the surface of the cylindrical opening created by the movement of the body C_4 (see Fig. 1). If there is a symmetry of manufacturing in the micro-valve, the movement of the body C_4 towards the left or towards the right yields the same at both points O_1 and O_2. Theoretically, the micro-valve body is assumed to be a perfect cylinder of radius R leading to the following expression of :

$$= 2nR(X - E) \tag{2}$$

As we supposed the friction is negligible, if the pressure P_d is assumed to be equal to P_0 and the pressure T_d is considered to be equal to the atmospheric pressure, then the pressure in chambers CH_{e1} and CH_{e2} is thus, $\frac{P_0}{2}$ in the rest position. According to the Bernoulli theorem, for a given point P_b of a fluid, it is possible to write the following relation:

$$\frac{V_{P_b}^2}{2} + \frac{P}{} + gh = C^{te} \tag{3}$$

where V_{P_b} is the fluid velocity at point P_b, P is its pressure at this point, represents the fluid volumic density, h is the height of the point P_b with regard to a given reference and g the gravity acceleration. By applying this theorem between both points O_1 and D_1 while assuming that these points are for the same height, the velocity of the fluid V_{D_1} at the point D_1 is give by:

$$V_{D_1} = \sqrt{\frac{2\,\mathbf{P}}{}} \tag{4}$$

As the micro-valve body begins to move towards the right, as the pressures in chambers CH_{e1} and CH_{e2} are no longer equal. The pressure is then equal to $((P_0/2) +)$ in the CH_{e1} chamber and to $((P_0/2) -)$ in the CH_{e2} chamber. represents the difference of the pressure created by the movement of the micro-valve body. Hence, the pressure difference P between both points O_1 and D_1 is given by: $\mathbf{P} = P_0 - \frac{P_0}{2} + = \frac{P_0}{2} - $ Moreover, using Vena Contracta constant, C, which is almost equal to 0.62, the flow Q_e created by the micro-valve can be defined by:

$$Q_e = C \cdot V_{D_1} \tag{5}$$

By substituting Eqs. (4) and (2) in Eq. (5), the flow Q_e can be established by:

$$Q_e = K_1(X - E)\sqrt{\frac{2((P_0/2) -)}{}} \tag{6}$$

with $K_1 = 2nCR$. The flow Q_e can also be established by using its definition and the fluid compressibility with a second relation as:

$$Q_e = S_e\dot{E} + V_e\dot{} \tag{7}$$

where $\dot{E}$ is the time derivative of the eccentricity E, V_e represents the CH_{e1} chamber's volume and is the compressibility coefficient defined as:

$$= -\frac{1}{V}\frac{\partial V}{\partial P} \tag{8}$$

V and P are, respectively, the volume and the pressure. For mineral fluid, this coefficient is almost equal to $1/16{,}000\ bar^{-1}$.

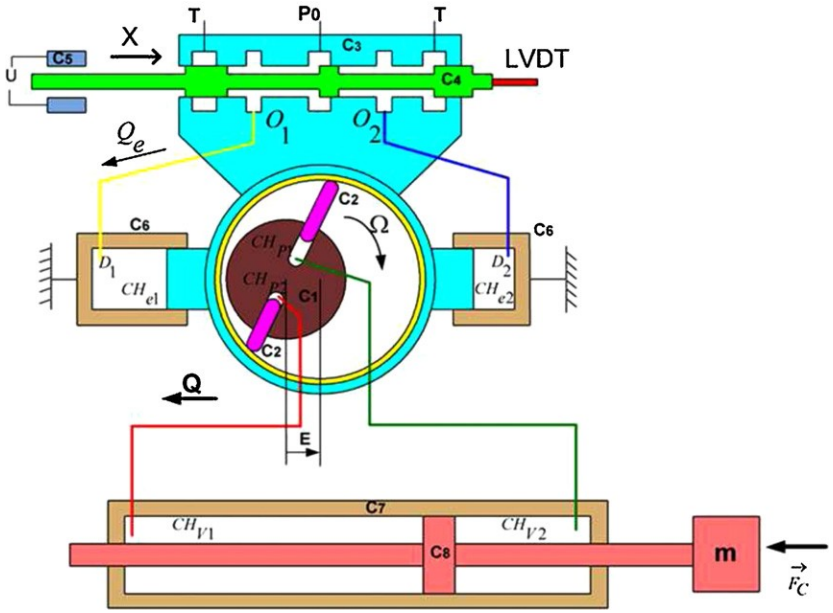

Fig. 1. IEHA simplified model (a linear actuator).

2.2. Micro-pump barrel dynamic equilibrium

The average flow value given by Eq. (1) can be also expressed by using the relation between the actuator linear output velocity $\dot{Y}$ and coefficient as:

$$Q = S_v\dot{Y} + V_v\dot{P}_{v1} \tag{9}$$

where S_v is the active section of the linear actuator, V_v is the CH_v chamber's volume and P_{v1} is the pressure in this chamber (see Fig. 1). Applying Newton's equation to the micro-pump barrel (C_3), with mass is m_e and acceleration of $\ddot{Y}_3$, all external forces can be identified. These forces, as depicted in Fig. 2, can be determined by the following:

1. Two forces produced by the fluid of the micro-valve stage on the barrel are $\vec{F}_{e1}$ and $\vec{F}_{e2}$.
2. Force exerted by the i th piston and induced by pressure P_{pi} in the corresponding chamber CH_{pi}. This force is given by $\vec{F}_{pi}$ and has a magnitude of S_pP_{pi}.
3. Gravity force which is perpendicular to the micro-pump shaft.

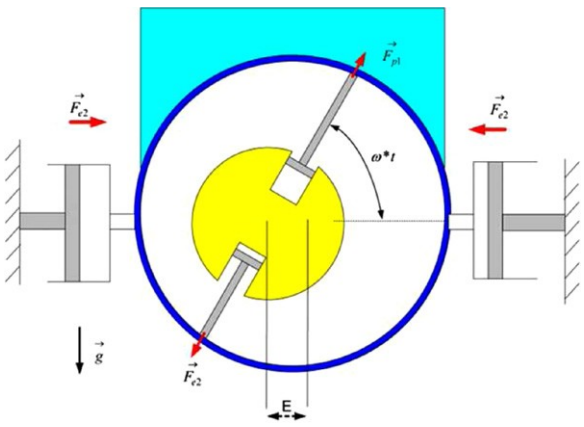

Fig. 2. Applied forces on the pump-barrel.

Hence, Newton's equation in its vectorial form can be expressed as follows:

$$m_e\ddot{Y}_3 = \vec{F}_{e1} + \vec{F}_{e2} + \vec{F}_{p1} + \vec{F}_{p2} + m_e\vec{g} \tag{10}$$

Using the pressures in both chambers CH_{e1} and CH_{e2}, the scalar projection of the above equation on the shaft axis leads to the following formulation:

$$m_e\ddot{E} = S_pP_{p1}\cos(\omega t) + S_pP_{p2}\cos(\omega t + n) + (P_0 + \Phi)S_e - (P_0 - \Phi)S_e \tag{11}$$

The later equation can take the following form:

$$m_e\ddot{E} = S_p(P_{p1} - P_{p2})\cos(\omega t) + 2\Phi S_e \tag{12}$$

2.3. Linear actuator dynamics

Applying Bernouilli theorem between the pistons located on the side of the micro-pump and the actuator chambers, for both cases, aspiration and expulsion leads to the following set of equations:

$$\frac{V_{p1}^2}{2} + \frac{P_{p1}}{} = \frac{\dot{Y}^2}{2} + \frac{P_{v1}}{} \tag{13}$$

$$\frac{V_{p2}^2}{2} + \frac{P_{p2}}{} = \frac{\dot{Y}^2}{2} + \frac{P_{v2}}{} \tag{14}$$

where V_{pi} is the fluid velocity in chamber CH_{pi}, which can be assumed to be equal to the linear velocity of the corresponding piston pi. Let us consider a simplified system with two pistons p_1 and p_2 (one in aspiration mode while the other in expulsion mode) and located, respectively, at $\theta_1 = \omega t$ and $\theta_2 = \omega t + n$. Hence, and for a given eccentricity $E = c^{te}$, the linear velocities V_{p1} and V_{p2} can be established by the time derivative of the pistons position L_p as follows[1]:

$$V_{p1} = +E\omega\sin(\omega t) - \frac{E^2\omega\sin(\omega t)\cos(\omega t)}{\sqrt{R_b^2 - E^2\sin(\omega t)^2}} \tag{15}$$

[1] Is clear that same results can be derived for each layer n_c, with odd number n_p^{max} of pistons for each.

$$V_{p2} = -E\omega \sin(\omega t) - \frac{E^2\omega \sin(\omega t)\cos(\omega t)}{\sqrt{R_b^2 - E^2 \sin(\omega t)^2}} \quad (16)$$

Going back to both Eqs. (13) and (14) and subtracting one from the other leads to:

$$\overset{\frown}{P}_v = \overset{\frown}{P}_p + \frac{1}{2}(V_{p2}^2 - V_{p1}^2) \quad (17)$$

This equation can be rewritten using both Eqs. (15) and (16), which gives the following non-linear equation:

$$\overset{\frown}{P}_v = \overset{\frown}{P}_p + 4\frac{E^3\omega \sin(\omega t)^2 \cos(\omega t)}{\sqrt{R_b^2 - E^2 \sin(\omega t)^2}} \quad (18)$$

The second term on the right side produces non-desired non-linearity, therefore, based on comparison between the various geometrical sizes, we established the following statement:

$$\frac{E}{R_b} < 1 \Rightarrow E\omega \sin(\omega t) \gg \frac{E^2\omega \sin(\omega t)\cos(\omega t)}{\sqrt{R_b^2 - E^2 \sin(\omega t)2}} \quad (19)$$

It is then possible to assert that $V_{p2} \approx -V_{p1}$, which leads us to establish the final form of the Bernoulli theorem for the pistons and the output actuator as follows:

$$\overset{\frown}{P}_v = \overset{\frown}{P}_p \quad (20)$$

Once again, applying Newton's equation to the payload, which its mass is equal to m while taking into account the external applied force F_c, leads to the following relationship:

$$m\ddot{Y} = S_v \overset{\frown}{P}_v - F_c \quad (21)$$

2.4. Input–output relation

Substituting Eqs. (20) and (21) into Eq. (12) gives the following formulation:

$$\frac{S_p}{S_v}(m\ddot{Y} + F_c)\cos(\omega t) + 2\Phi S_e = m_e \ddot{E} \quad (22)$$

Since our objective is to establish the relation between the input X and the output Y, it is necessary to get the following expression of Φ from the above Eq. (22):

$$\Phi = K_2\ddot{E} - K_3\ddot{Y}\cos(\omega t) - K_4 F_c \cos(\omega t) \quad (23)$$

where constants K_i, i = 2, 3, 4 are introduced in order to simplify the notations:

$$K_2 = \frac{m_e}{2S_e}, \qquad K_3 = m\frac{S_p}{2S_e S_v}, \qquad K_4 = \frac{S_p}{2S_e S_v} \quad (24)$$

The time derivative of Eq. (21) combined with the expression of $\dot{\overset{\frown}{P}}_v$ leads to:

$$\dot{P}_{v1} = \frac{m}{2S_v}Y^{(3)} + \frac{\dot{F}_c}{2S_v} \quad (26)$$

$Y^{(k)}$ is the k th time derivative of Y (i.e. $Y^{(3)}$ is the pay-load jerk). Let us assume that the output actuator initial position is in the middle of its stroke and its total length is L_0. In that case, the volume of the chamber is given by:

$$V_v = \frac{L_0}{2} + Y \quad S_v \quad (27)$$

This leads us to formulate Eq. (25) as:

$$E = K_5\dot{Y} + mK_6 Y^{(3)} + K_6\dot{F}_c + mK_7 Y\ddot{Y}^{(3)} + K_7 Y\dot{F}_c \quad (28)$$

where constants K_i, i = 5, 6, 7 are introduced for the above mentioned reason:

$$K_5 = \frac{S_v}{2N_p S_p Q}, \qquad K_6 = \frac{L_0}{8N_p S_p Q}, \qquad K_7 = \frac{}{4N_p S_p Q} \quad (29)$$

If we consider that the micro-pump shaft is rotating at almost constant speed (ω ◆ C^t), then the following relationship can be written:

$$\dot{E} = K_5\ddot{Y} + mK_6 Y^{(4)} + K_6\ddot{F}_c + mK_7\dot{Y}Y^{(3)} + mK_7 Y\ddot{Y}^{(4)} + K_7\dot{Y}F_c + K_7 Y\ddot{F}_c \quad (30)$$

Taking the time derivative of the above equation leads to the expression of the micro-pump barrel's acceleration $\ddot{E}$, which can be established as follows:

$$\ddot{E} = K_5 Y^{(3)} + mK_6 Y^{(5)} + K_6 F_c^{(3)} + mK_7\ddot{Y}Y^{(3)} + mK_7\dot{Y}Y^{(4)} + mK_7\dot{Y}Y^{(4)} + mK_7 Y\ddot{Y}^{(5)} + K_7\ddot{Y}\ddot{F}_c + K_7\dot{Y}\ddot{F}_c + K_7\dot{Y}\dot{F}_c + K_7 Y F_c^{(3)} \quad (31)$$

On the other hand, the leakage in the chambers (CH_{ei}, i = 1, 2) can be neglected since their volume is smaller than of the output actuator chambers. By substituting Eqs. (23) and (7) in Eq. (6), the later can be rewritten in the following form:

$$S_e\dot{E} = K_1(X - E) \quad \sqrt{\frac{P_0}{2} - K_2\ddot{E} + K_3\ddot{Y}\cos(\omega t) + K_4 F_c \cos(\omega t)} \quad (32)$$

A non-linear relationship links an implicit form of the input X to the output Y through the times derivative of Y and the external force F_c applied to the pay-load. To get the full expression, one can replace the above equation by the internal variable E (Eq. 28) and its first and second time derivatives $\dot{E}$ and $\ddot{E}$ given, respectively, by Eqs. (30) and (31). This leads to a complex relation, which is the base of the simulation carried out in the following section.

$$K_5\ddot{Y} + mK_6 Y^{(4)} + K_6\ddot{F}_c + mK_7\dot{Y}Y^{(3)} + mK_7 Y\ddot{Y}^{(4)} + K_7\dot{Y}\dot{F}_c + K_7 Y\ddot{F}_c = \frac{K_1}{S_e}(X - K_5\dot{Y} + mK_6 Y^{(3)} + K_6 F_c + mK_7 Y\ddot{Y}^{(3)} + K_7 Y\dot{F}_c) \times \sqrt{\frac{P_0}{2} - K_2K_5 Y^{(3)} - mK_2K_6 Y^{(5)} - K_2K_6 F_c^{(3)} - mK_2K_7\ddot{Y}Y^{(3)} - mK_2K_7\dot{Y}Y^{(4)} - mK_2K_7 Y\ddot{Y}^{(5)} - K_2K_7\ddot{Y}F_c - K_2K_7\dot{Y}\ddot{F}_c - K_2K_7\dot{Y}\dot{F}_c - K_2K_7 Y F_c^{(3)} + K_3\dddot{Y}\cos(\omega t) + K_4\ddot{F}\cos(\omega t)} \quad (33)$$

When the micro-pump stage starts moving the output actuator from its equilibrium position, the pressure in both chambers CH_{v1} and CH_{v2} will change symmetrically allowing us to admit that $P_{v1} = -P_{v2}$ or even more $\overset{\frown}{P}_v = 2P_{v1}$. Hence, using Eqs. (1) and (9), the eccentricity E can be expressed as follows:

$$E = \frac{S_v}{2N_p S_p Q}\dot{Y} + \frac{V_v}{2N_p S_p Q}\dot{P}_{v1} \quad (25)$$

3. Simulation results

Given the complexity of the proposed system, to achieve a globally optimised solution it is important to proceed in an iterative manner. This iterative process is coupled with analyses by simulations of a virtual model and experimental measurements taken with a built prototype (described in the next section). The IEHA theoretical performances are established taking advantage of the

simulation results based on the relationships developed in previous section. The aim of the carried out simulations is to allow us to quantify the contributions of each IEHA stages (micro-pump, micro-valve and passive distributor). The forward objective of this simulation is double in the sense that it consists of comparisons between the simulated performances and the real measurements. Providing suggestions for improvements of the physical prototype, as well as, refinements of the several models included in the simulator. To this aim, two simulation models under Matlab-Simulink were developed. The relatively simplistic one has the objective of reproducing the functioning of the IEHA open-loop. The second aims at quantifying the IEHA behavior when closed loop control is carried out with sensors signals.

3.1. Open-loop model

As discussed in the previous section, the IEHA input–output relationship is a non-linear fifth order differential equation linked to the micro-valve position X and to the linear actuator position Y. The first simulation model is built by reducing the study to the simple case without taking into account the compressibility of the fluid. Fig. 3 presents a block diagram of the implemented simulator. In this model, the micro-valve block is built using two inputs X and ♦ and an output which is the eccentricity E. Eq. (6) giving the flow Q_e in the case of neglecting the fluid compressibility is implemented in this block.

$$Q_e = 2\tilde{C}R(X - E)\sqrt{2((P_0/2) - \blacklozenge)} \quad (34)$$

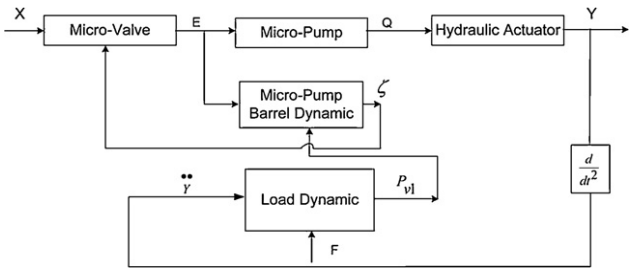

Fig. 3. IEHA simplified simulation model.

The micro-pump block presents the stage of hydraulic energy production implemented using Eq. (1), providing the average flow Q. Its input is the eccentricity E while its output is the above mentioned flow Q. By neglecting the fluid compressibility, the block simulate a linear actuator with the payload based on the following new Eq. (9). This simulation block has as input the flow Q and as output Y.

$$Q = S_v\dot{Y} \quad (35)$$

The dynamics of micro-pump barrel is implemented according to Eq. (12), in the simulation block with two inputs: the main one which is the eccentricity E and an auxiliary input providing the pressure of the first chamber of the linear actuator P_{v1}. The output of this block is the pressure of the chamber of the micro-pump barrel ♦. The auxiliary input is taken from the linear actuator's chamber, as the pressure loss between the micro-pump and the linear actuator can be neglected (see Eq. (20)). As the passive distributor always guarantees that the connection of the return of the linear actuator

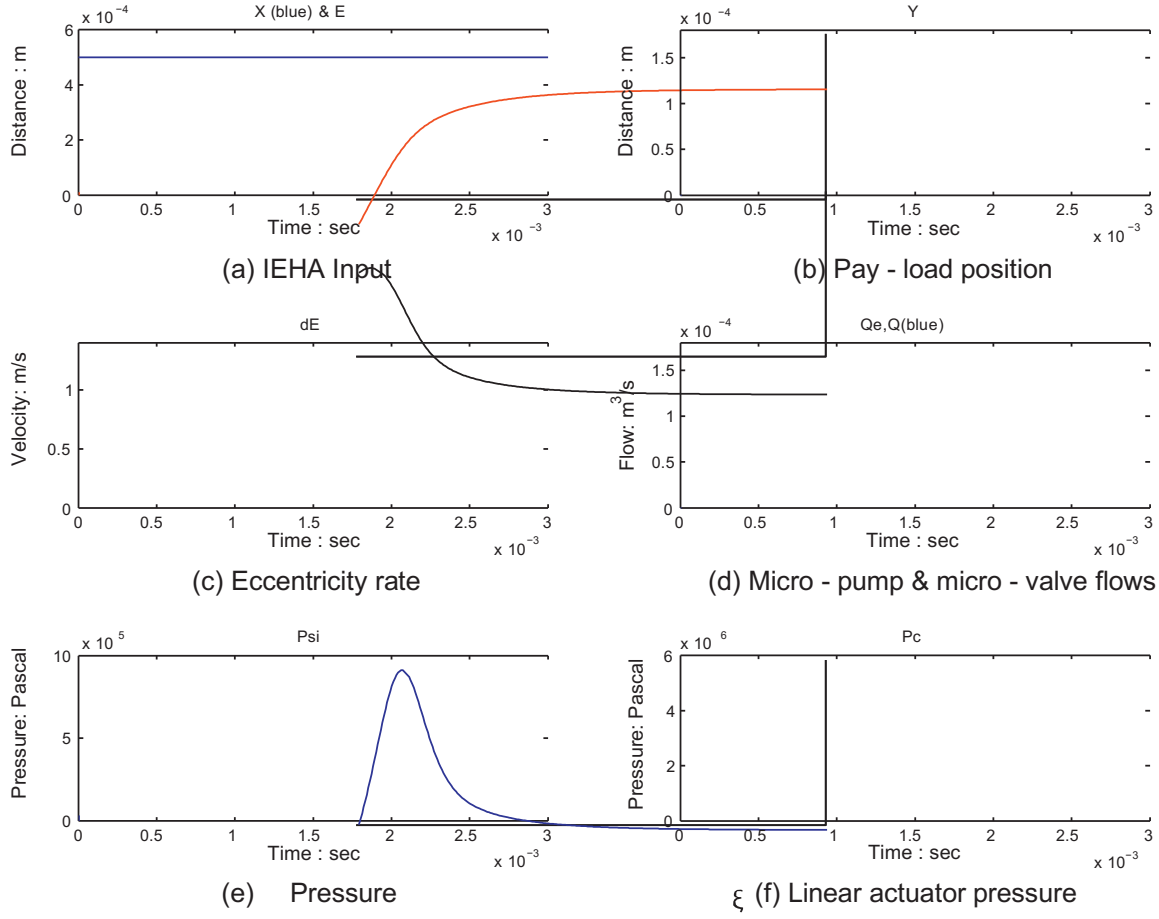

Fig. 4. Open-loop simulation results for an input step X.

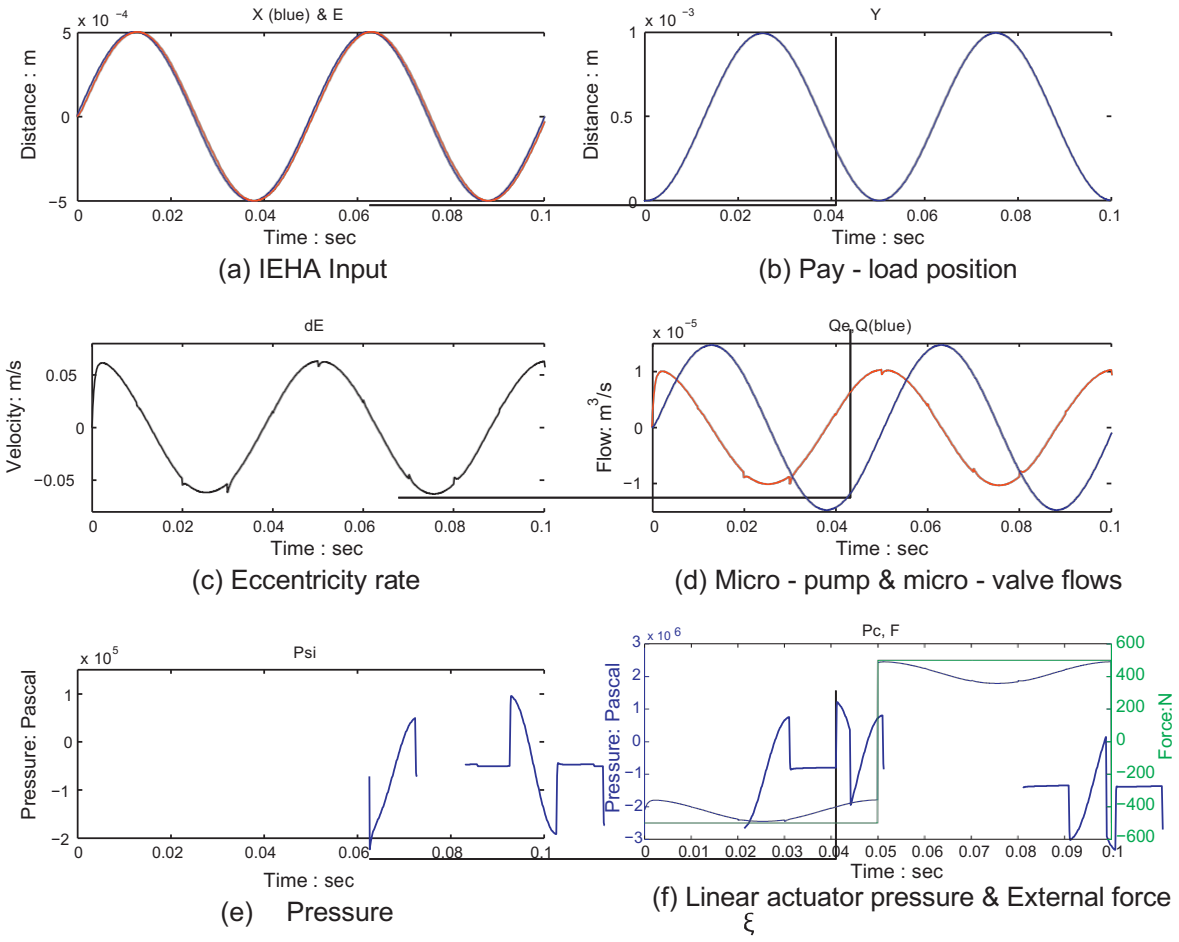

Fig. 5. Open-loop simulation results for external applied force.

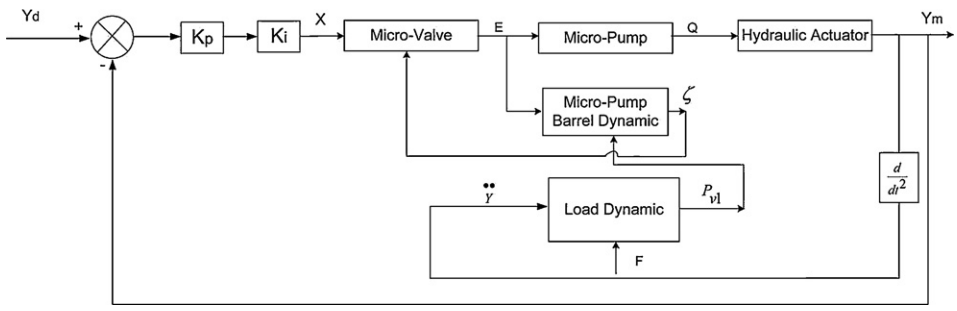

Fig. 6. IEHA closed loop simulation model.

P_{v2} is equal to the atmospheric pressure. Hence, the pressure P_{v2} can be neglected, allowing us to define the considered block using the following equation:

$$m_e \ddot{E} = S_p P_{v1} \cos(\omega t) + 2\diamondsuit S_e \tag{36}$$

The last simulated block is concerned with the dynamics of the payload m, it has two main inputs $\ddot{Y}$ and F_c and a single output, which is the pressure P_{v1}. It is implemented using Eq. (37):

$$m\ddot{Y} = S_v P_{v1} - F_c \tag{37}$$

Once all the simulation blocks are defined, the links between inputs and outputs are realised as shown in Fig. 3. Table 1 provides the values of the parameters used in the developed simulation model.

Table 1
Parameters values used in the open-loop simulation.

Parameter	Physical meaning	Value
m	Payload mass	10 kg
S_v	Linear actuator active surface	2.35 cm^2
F	External force applied to the payload	0 N
m_e	Micro-pump barrel mass	0.09 kg
n_p	Number of pistons	15
S_p	Surface of the piston	0.19 cm^2
S_e	Micro-pump barrel active surface	1.64 cm^2
E_{max}	Maximal eccentricity	0.05 cm
r_{tig}	Micro-valve radius	0.25 cm
ω	Shaft speed	3000 rpm
C	Vena Contracta coefficient	0.62
	Fluid density	840 kg/m^3
P_0	Micro-valve input pressure	10^5 Pa

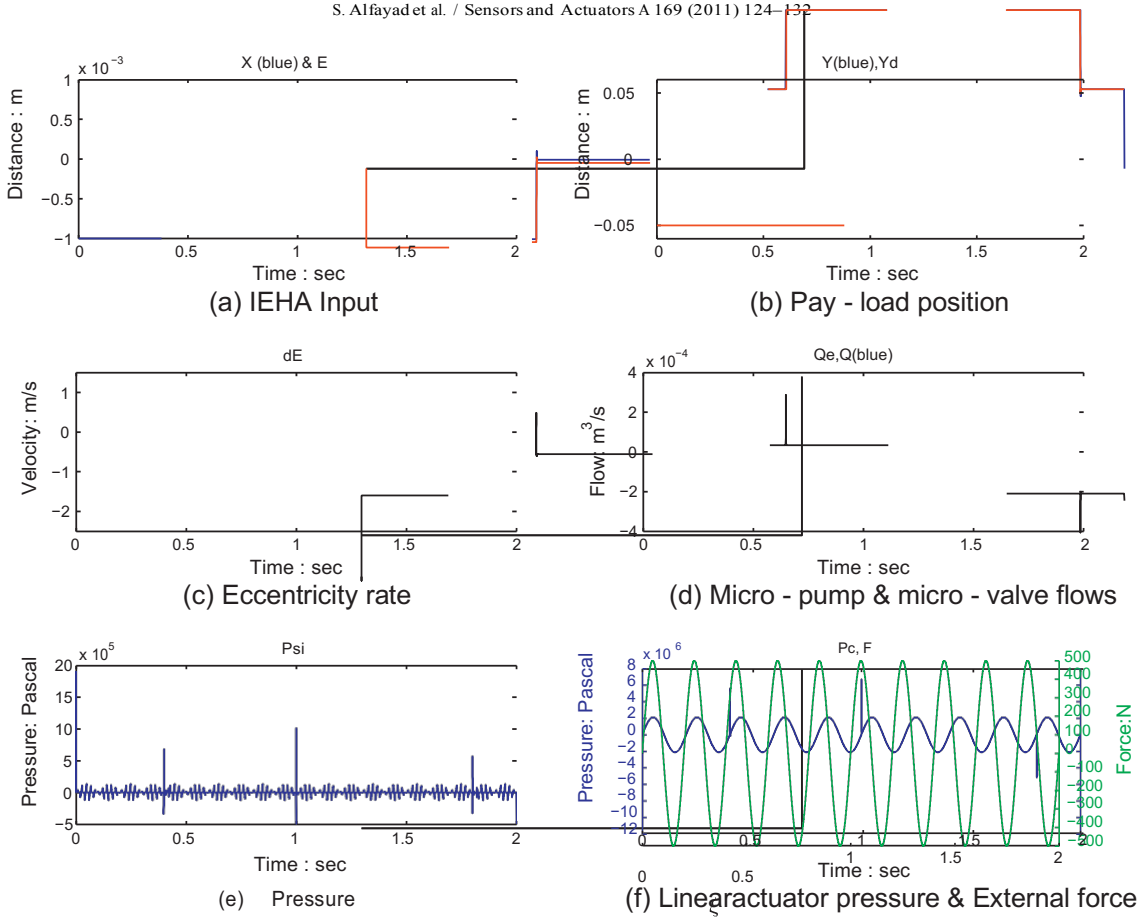

Fig. 7. Closed loop simulation results with external force and $X_{max} = 1$ mm.

3.2. Open-loop simulation results

Fig. 4 provide the results obtained from open-loop simulations. The input signal is at steps of 0.5 mm corresponding to the variable X controlling the position of the micro-valve. Since it is an open-loop simulation, the output Y increases infinitely and this for an eccentricity fixed to a maximal value. The time response of the micro-valve is almost of 1.5 ms. In this first simulation, no force is applied to the payload. This explains that the pressure converges to zero, as the payload's acceleration nullified.

The second simulation is carried out by applying a sinusoidal input with a period of 50 ms and of an amplitude of 0.5 mm. A periodic external force is also applied to the payload. This force has a period of 100 ms and an amplitude of 40 kg. Fig. 5 shows the resulting response of the system, which demonstrates clearly that the proposed IEHA has two intrinsic feedback loops. The first loop exists between the input X and the eccentricity E, while the second links the external applied force F_c to the pressure produced by the micro-pump P_{v1}.

3.3. Closed loop control

To be able to control the linear actuator output Y, a LVDT displacement sensor is used to measure the micro-valve position. A closed loop with a Proportional and an Integral terms are incorporated into the simulation model developed. The new simulation model is shown in Fig. 6. The values of the proportional and integral gains (k_p, k_i) are adjusted to have an acceptable time response. The values obtained after several trials are $k_p = 0.01$ and $k_i = 0.3$ (other parameters are given in Table 1). Fig. 7 shows that the system's time response is almost equal to 400 ms. By analysing the variation of the input X and of the eccentricity E over time, a very low latency between these two variables appears. Nevertheless, both variables remain for a long time equal to their maximum values. This is probably due to the fact that the simulated micro-valve is not large enough.

By using a micro-valve with a bigger stroke ($X_{max} = 1.5$ mm), the time response is reduced to 100 ms, with the same values of the above mentioned gains ($k_p = 0.01$ and $k_i = 0.3$). Fig. 8 shows the new results. An alternative way to improve the time response of the system consists of increasing the micro-valve diameter which would increase its section, and hence, its dynamics.

4. Comparisons with experimental results

In order to carry out experimental results, the test-bed device dedicated to the IEHA [1] is used. This test-bed allows us to carry out continuously several experiments as detailed in the following sections:

4.1. Experiment 1: flow evolution with the rotation speed

Fig. 9 shows the flow variation produced by the IEHA according to the rotation speed of the input electric motor. Two curves are drawn on this figure. The first one (in black) concerns the theoretical flow calculated by means of the Eq. (1); the second (in magenta) is relative to the real flow measured by the test-bed (For interpretation of the references to color in this figure, the reader is referred to the web version of the article.). The difference between the experimental and theoretical results is greatest at low rotation speeds. This difference tends to decrease when the rotation speed of the input electric motor increases. This phenomenon is caused by the decrease of the centrifugal forces when the rotation speed decreases. The result demonstrated in this experiment

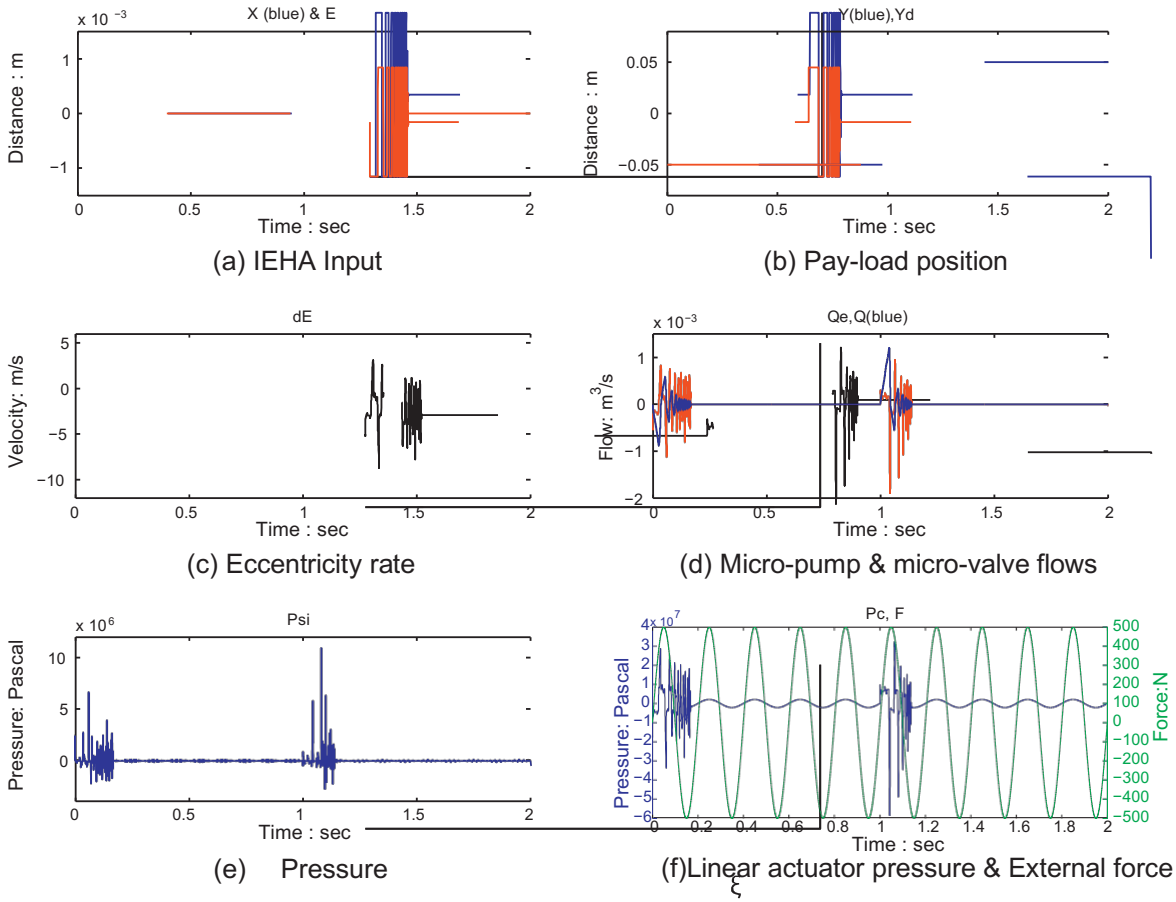

Fig. 8. Closed loop simulation results with external force and X_{max} = 1.5 mm.

shows that there is an "optimal" rotation speed for which the centrifugal forces applied to pistons are big enough to allow these to accomplish their over-all displacement, and hence, to make the real flow rate to approach the theoretical value. Going over this optimal rotation speed, the increase of the flow is very low regards to the drawbacks related to the noise generated by the high speed. Practically, the optimal rotation speed is identified for this prototype around 3000 rmp.

4.2. Experiment 2: relation between the output pressure and the produced flow

In this experiment, the rotation speed ω is fixed at 3000 rpm. The eccentricity E is equal to 0.13 mm and the number of used pistons is equal to 15. Every piston has a radius of in 0.25 mm. By changing the position of the flow reducer, the IEHA feels its payload increasing with an increase of its output pressure. Fig. 10 gives the flow variation produced for several values of output pressure (i.e. the payload), the two curves shown are: a theoretical one (in black) and the experimental one (in magenta) (For interpretation of the references to color in this figure, the reader is referred to the web version of the article.). The results show that when the output pressure increases, the produced flow decreases, and the distance between the real and theoretical values increases. Since all the characteristics of the actuator (E, N_p and ω) are fixed, the flow lost takes place inside the IEHA due the internal leakages. This issue will be improved in the future planned prototypes.

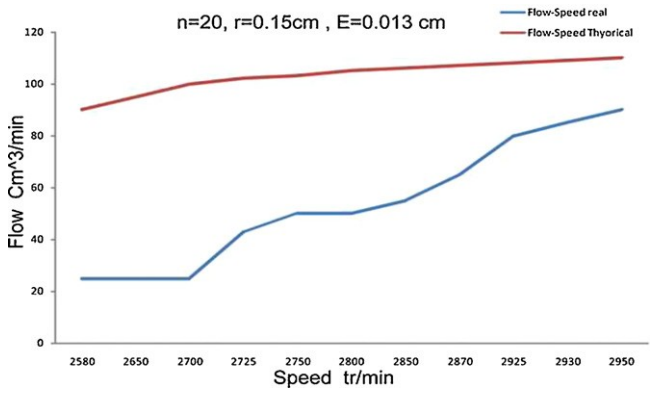

Fig. 9. Preliminary results showing the flow variation versus the rotation speed.

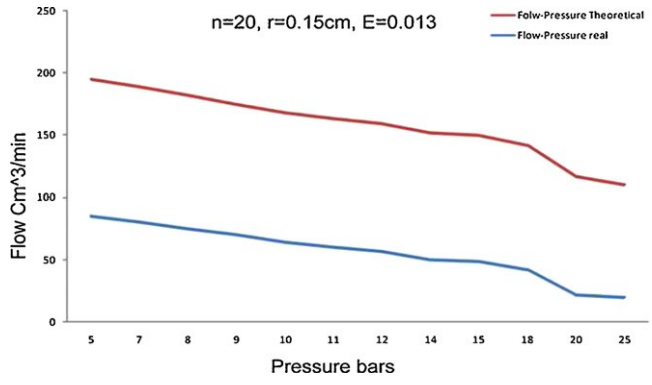

Fig. 10. Preliminary results giving the output pressure versus the produced flow.

5. Conclusion

In this paper, the new Integrated Electro-Hydraulic Actuator (IEHA) was modeled base on several subsystems (micro-pump, micro-valve and passive distributor) detailed in the first part of this work. The theoretical input/output relation between the positions of the micro-valve X and the payload Y was established using the dynamics of each subsystem. This theoretical modelling leads to a fifth order non-linear differential equation showing our ability to access to several time derivatives of the payload position. A set of simulation for open and closed loop functioning were carried out based on the Matlab-Simulink models developed. This allowed us to establish several interesting results concerning the time response and the needed maximum value of the micro-valve position. In order to validate the concept, several experiments giving the variation of the flow and the pressure function of the eccentricity were carried out using a IEHA prototype and a hydraulic test-bed. Further works concerning the improvements of the IEHA performances are planned, such as pressure, flow and speed are currently under development. The ultimate goal of theses developments will be to closely emulate the behaviours of an artificial muscle with intrinsic active compliance properties.

Acknowledgment

This work is part of a research project funded by the French National Agency for Research (ANR).

References

[1] S. Alfayad, F.B. Ouezdou, F. Namoun, G. Cheng, High performance integrated electro-hydraulic actuator for robotics. Part I: Principle, prototype design & first experiments, Sensors and Actuators A: Physical (2010).
[2] J.E. Bobrow, J. Desai, A high torque to weight ratio robot actuator, Robotica 13 (1995) 201–208.
[3] S. Habibi, Design of new high-performance electrohydraulic actuator, IEEE/ASME Transactions on Mechatronics 5 (2) (2000) 158–164.
[4] S. Habibi, R. Burton, E. Smapson, High precision hydrostatic actuation systems for micro-and nanomanipulation of heavy loads, Journal of Dynamic Systems, Measurement, and Control 128 (4) (2006) 778–787.
[5] A. Kargov, T. Werner, C. Pylatiuk, S. Schulz, Development of a miniaturised hydraulic actuation system for artificial hands, Sensors and Actuators A: Physical 141 (2) (2008) 548–557.
[6] H. Kaminaga, T. Yamamoto, J. Ono, Y. Nakamura, Backdrivable miniature hydrostatic transmission for actuation of anthropomorphic robot hands, in: IEEE-RAS International Conference on Humanoid Robots, 2007.
[7] H. Kaminaga, J. Ono, Y. Nakashima, Y. Nakamura, Development of backdrivable hydraulic joint mechanism for knee joint of humanoid robots, in: IEEE International Conference on Robotics and Automation, 2009.
[8] J.M. Winters, L. Stark, Analysis of fundamental movement patterns through the use of in-depth antagonistic muscle models, IEEE Transactions on Biomedical Engineering BME-32 (1985) 826–839.
[9] Macrosensors, Lvdt Basics, 2010. Available from: http://www.macrosensors.com/downloads/misc/primer.013103.pdf.

Biographies

Dr. Samer Alfayad is currently a Post-doc fellowship at University of Versailles. He received his M.S. from the Ecole Nationale Supérieure des Arts & Métiers and Ph.D. degrees from the University of Versailles Saint Quentin (UVSQ), in 2005 and 2009, respectively. He was graduated from Engineering School in Mechatronics (ISSAT, Syria) in 1999. From 1999 to 2004, he was Associate Professor at ISSAT.

Prof. Fethi B. Ouezdou is currently a Full Professor in the Physics and Mechanics Department of the University of Versailles St. Quentin en Yvelines. He is the leader of Interactive Robotics group in the LISV Laboratory. He received his M.S. from the Ecole Nationale Supérieure des Arts & Métiers and Ph.D. degrees from the University of Pierre et Marie Curie (Paris 6), in 1986 and 1990, respectively. From 1990 to 1991, he was Researcher at the University Paris 6, and worked on the project of quadruped locomotion. From 1991 to 2004, he was an Associate Professor, at the University of Versailles and holds Position at the Department of Mechanical Engineering of the University of Versailles. He was also the head of the Department.

Faycal Namoun is the Founder (in 1986) and main officer of BIA Company. He obtained his M.S. from the Ecole Nationale Supérieure des Arts & Métiers. Specialist worldwide recognized in hydraulics and fast advanced motion control. With 24 years of experience in automotive and aeronautics field. He is inventor/co-inventor of six patents and several concepts used daily in the automotive and aerospace environments.

Prof. Gordon Cheng is the Chair of Cognitive Systems, Founder and Director of Institute for Cognitive Systems at the Technical University of Munich (TUM), Germany. He was the Head of the Department of Humanoid Robotics and Computational Neuroscience (2002–2008), ATR International, Kyoto, Japan. He was the Group Leader (2003–2008) for the JST ICORP, Computational Brain Project. He was also designated as a Project Leader (2007–2008) for National Institute of Information and Communications Technology (NICT) of Japan. He held fellowships from the Center of Excellence (COE), Science and Technology Agency (STA) at the ElectroTechnical Laboratory (ETL), Japan.